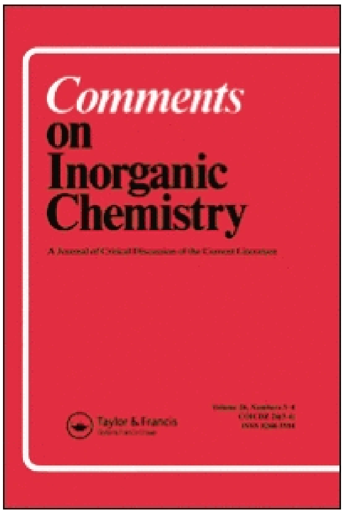

Comments on Inorganic Chemistry
Publication details, including instructions for authors and subscription information:
http://www.informaworld.com/smpp/title~content=t713455155

Site Preference Effects in Heterometallic Clusters

D. Michael[a]; P. Mingos[a]; Lin Zhenyang[a]
[a] Inorganic Chemistry Laboratory, University of Oxford, Oxford, United Kingdom

To cite this Article Michael, D. , Mingos, P. and Zhenyang, Lin(1989) 'Site Preference Effects in Heterometallic Clusters', Comments on Inorganic Chemistry, 9: 2, 95 — 122
To link to this Article: DOI: 10.1080/02603598908035805
URL: http://dx.doi.org/10.1080/02603598908035805

Site Preference Effects in Heterometallic Clu

D. MICHAEL P. MINGOS and LIN ZHE
Inorganic Chemistry L
University of Oxford, South P
Oxford OX1 3QR, Unite

In organometallic chemistry new and versatile synthetic routes have been
for isolating heterometallic ligated cluster compounds with up to 44 me
Naked mixed metal clusters with size ranges of 10–50 Å are of imp
catalytic processes and smaller naked heterometallic clusters have been
molecular beam experiments. These rather different areas raise commo
concerning the relative dispositions of the two types of metal atoms. In
a general analysis of site preference effects derived from molecular orbi
bation theory methods is developed. For naked clusters the site prefe
controlled primarily by the relative strengths of the metal–metal bond
metal that forms stronger metal–metal bonds occupying interstitial or
nectivity sites. For ligated clusters these effects are important but t
strengths of the metal–ligand bonds can also play a decisive role.

Key Words: *clusters, heterometallic clusters, site preferences in heterome*
ters, theoretical studies on clusters, naked clusters, ligated clusters

INTRODUCTION

Clusters have become the subject of an increasing numbe
oretical and experimental investigations because of their p
as models for catalytic processes which occur on metal cry
and as catalysts in their own right.[1-3] Clusters can be c

Comments Inorg. Chem.
1989, Vol. 9, No. 2, pp. 95–122
Reprints available directly from the publisher
Photocopying permitted by license only

into two major groups—naked and ligated clusters. As the names imply, ligated clusters are molecular compounds derived from naked clusters by the coordination of ligands (e.g., carbonyls, halides and phosphines) to their surface atoms. Naked clusters of metals are generally studied in molecular beam and matrix isolation experiments under conditions which prevent aggregation reactions to the bulk metal.[4,5] In addition larger metal cluster fragments are formed on oxide supports and are important as heterogeneous catalysts.[6] Theoretical studies on clusters have concentrated largely on their structures and stabilities. The geometries of ligated cluster compounds have been rationalized by a set of simple rules described collectively as the Polyhedral Skeletal Electron Pair Theory[7] which has been underpinned by Stone's Tensor Surface Harmonic Theory.[8] A corresponding general theory for the understanding of the bonding in naked clusters has not yet emerged although quantum mechanical methods have been used to understand the details of the orbital energies, electronic structures, ionization energies and geometries of some specific clusters.[9,10] In addition, a simple Jellium Model has been developed by Knight *et al.*, to account successfully for the occurrence of magic numbers in the mass spectra of naked alkali metal clusters.[11]

Although numerous studies on the structural aspects of clusters have been computed, less attention has been paid to the site preferences of atoms in mixed clusters. For example, for a cluster with an interstitial moiety, the relative locations of metal atoms on the interior or on the surface of the cluster are particularly important for understanding the activities of bimetallic or multimetallic catalysts. In this paper, we describe some general principles governing these site preferences and discuss the influence of ligands on these site preferences. For surface segregation in binary solid solutions a theory based on thermodynamic considerations has been developed which takes into account surface bond breaking and bulk strain energies.[12]

STRUCTURAL ASPECTS

Mixed Naked Clusters

Mixed metal clusters with size ranges of 10–50 Å are particularly important in catalysis.[6] One important groups contains a combination of atoms of a group VIII(8–10) metal and a group IB(11) metal (numbers in brackets indicate the number of valence electrons), for example, Ru–Cu and Os–Cu clusters. Another interesting group of bimetallic clusters has a combination of atoms of two group VIII(8–10) metals, such as Ir–Pt and Ir–Rh clusters, or a combination of two group IB(11) metals, e.g., Cu–Ag and Cu–Au clusters. Although the two metals are miscible to some extent in the bimetallic clusters, it has been found that the surface sites in the clusters are preferentially occupied by some metals, whereas the interior sites preferentially by the others. The structural data[6] which have been obtained from the results of EXAFS analyses are summarized below:

Bimetallic Clusters	Interior Region	Surface Region
Re–Cu	Re–rich	Cu–rich
Ru–Cu	Ru–rich	Cu–rich
Rh–Cu	Rh–rich	Cu–rich
Re–Cu	Re–rich	Cu–rich
Os–Cu	Os–rich	Cu–rich
Ir–Cu	Ir–rich	Cu–rich
Pt–Cu	Pt–rich	Cu–rich
Ir–Rh	Ir–rich	Rh–rich
Re–Pd	Re–rich	Pd–rich
Re–Pt	Re–rich	Pt–rich
Cu–Ag	Cu–rich	Ag–rich

It is noteworthy that the surface composition of bimetallic clusters can be influenced by the gaseous atmosphere in contact with the clusters. For example, the location of the Au-rich region in the Au–Cu clusters is less clear from the EXAFS data, but there is a slight indication that it is present at the surface in a hydrogen atmosphere.[13] The presence of impurities such as sulfur and carbon can change the site preferences leading to a situation where the Cu concentrates at the surface.[13] Such a phenomenon is also observed for metal alloys. In the Ag–Pd and Au–Pd alloys,[14] the surface in ultrahigh vacuum is found to be enriched with Ag and Au. However, the surface becomes enriched with Pd upon prolonged contacted with CO at 293 and 373 K. This process can be reversed by removing the CO under high vacuum at 573 K. The same phenomenon is found for Ni–Au alloys.[15]

For small mixed naked clusters, attention has been focussed on the K_nMg and KNa_n, etc., clusters generated in molecular beam experiments and probed by photoionization mass spectroscopy.[16] Although the details of their structures have not been obtained experimentally, *ab initio* theoretical investigations on K_nMg and K_nAl clusters have indicated that Mg and Al atoms occupy preferentially the interstitial sites in such clusters.[10]

Mixed Ligated Clusters

For small clusters with 6–11 surface skeletal atoms, the interstitial moiety is usually a main group atom, e.g., $Ru_6C(CO)_{17}$ (octahedron, C at the center)[17] and $[Rh_{10}S(CO)_{22}]^{2}$ (bicapped square antiprism, S at the center).[18] For clusters with 12 surface skeletal atoms, the interstitial atom can be either a larger main group atom or a metal atom, e.g., $[Rh_{12}Sb(CO)_{27}]^{3}$ (icosahedron, Sb at the center)[19] and $[Rh_{12}Pt(CO)_{24}]^{4-}$ (anti-cuboctahedron, Pt at the center).[20] Only a few examples of larger mixed metal clusters have been characterized structurally. The largest clusters known at present are $[H_2Ni_{38}Pt_6(CO)_{48}]^{4-}$ and $[HNi_{38}Pt_6(CO)_{48}]^{5-}$ which have the aesthetically beautiful 44 atom octahedron based on fcc (face centered cubic close packed) arrangement.[21] The six platinum atoms form an inner octahedron in the interior of the cluster. Other examples exist where the central moiety is not completely encapsulated. For example, the hexacapped octahedral cluster $[H_3Fe_6Pd_6(CO)_{24}]^{3-}$ has the six Pd atoms forming an inner octahedron.[22] The two uncapped faces of the octahedron are trans to each other so that the cluster approximates to two close packed layers. The single crystal X-ray crystallographic data and, where available, solution nmr studies have indicated that the observed site preferences are determined by significant energy barriers, i.e., there is no evidence for disorder or intramolecular scrambling in these compounds.

The different sites can have very different connectivities in the clusters. The differences in connectivities in simple spherical clusters are smaller than those in clusters where atoms lie on several layers. For example, in trigonal and pentagonal bipyramidal clusters, the connectivities for the axial and equatorial atoms differ by only one. For multilayer spherical structures, the differences are larger, e.g., in $[H_2Ni_{38}Pt_6(CO)_{48}]^{4-}$, the connectivities range from 4 to 12.[21]

THEORETICAL MODELS

Differences in the electronegativities of main group atoms have been widely used for discussing the site preference of a heteroatom in heteroconjugated organic molecules[23] and deltahedral heteroboranes.[24] Theoretically these preferences have been interpreted using first-order perturbation theory arguments. Within the Hückel approximation, the total π-energy for a homoconjugated molecule is[25]:

$$E = \sum_{i} q_i \alpha_i + 2 \sum_{i<j}\sum p_{ij}\beta_{ij}$$

where q_i is the π-electron density of ith atom, p_{ij} is the Mulliken bond order between ith and jth atoms, α_i and β_{ij} are the corresponding Coulomb and resonance integrals. In a heteroconjugated molecule, the effect of the change in the heteroatom k is to alter the integrals α_k and β_{kl}. The change in the total energy due to the changes in α_k to $\alpha + \delta\alpha$ and β_{kl} to $\beta + \delta\beta$ is given by perturbation theory:

$$\delta E = q_k \delta\alpha + 2 \sum_{l} p_{kl} \delta\beta$$

The term $\alpha + \delta\alpha$ is determined primarily by the electronegativity difference between the heteroatom and carbon, and $\beta + \delta\beta$ by differences in bonding capabilities of the heteroatom and carbon.

In the discussion of heteroconjugated organic molecules[23] and heteroboranes[24] the electronegativity effect is usually considered as the dominant one and $\delta\beta$ is usually assumed to be zero. The stabilization energy δE is then given by:

$$\delta E = q_k \delta\alpha$$

It can be concluded from the equation above that those atoms which are more electronegative prefer to occupy positions which bear a larger negative charge in the parent polyene or polyhedron.

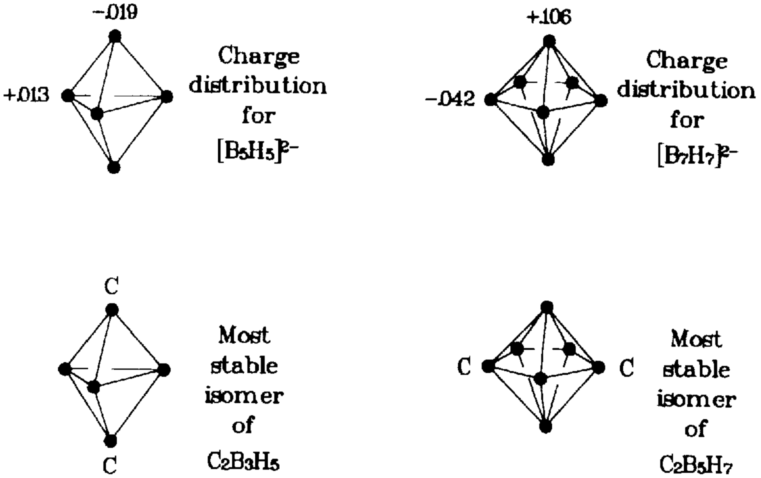

FIGURE 1 The charge distributions for $[B_5H_5]^{2-}$ and $[B_7H_7]^{2-}$, and the most stable isomers of $C_2B_3H_5$ and $C_2B_5H_7$ molecules.

These arguments have been adapted successfully to account for the relative stabilities of carborane cluster molecules.[24] For example, the most stable $C_2B_3H_5$ and $C_2B_5H_7$ carboranes illustrated in Fig. 1 correspond to the positions of greatest electron density in the parent borane anions, $B_5H_5^{2-}$ and $B_7H_7^{2-}$. The computed charges for these geometries shown in the figure clearly show a reversal in the relative distribution of negative charge between equatorial and axial sites. Since carbon is more electronegative than boron the greatest stabilization energies are obtained for the observed isomers.

When the electronegativity differences are smaller ($\delta\alpha \approx 0$) then the dominant term arises from $\delta\beta$. This is likely to be a more realistic model for clusters derived from heavy main group atoms or containing transition metals adajacent in the Periodic Table. In these situations the site preferences depend on the difference in metal–metal interactions for different atoms ($\delta\beta$). The first order correction to the total energy arising from a change in resonance integral from β to $\beta + \delta\beta$ of atom k is given by:

$$\delta E = 2\sum_{l} p_{kl}\delta\beta_{kl}$$

The summation runs for all atoms except the kth atom. The implications of this perturbation theory expression for discussing the site preferences in clusters is discussed in the following sections.

Naked Clusters

In order to highlight the important features a simple model structure is considered which is based on a centered cuboctahedral structure (**1**) with an fcc (face centered close packed) structural arrangement. The model is based initially on a cluster where the bonding involves metals having one s orbital per atom. Some of the important aspects of the real (all valence orbital interaction) case will be missed in a study of the s orbital model, but the analysis does yield some results of general applicability.

The symmetry-adapted linear combinations of these $|s_i\rangle$ functions can be expressed in terms of the following spherical harmonic expansion[7]:

$$\Psi_{lm}(s) = N' \sum_{i} C_{lm}(\theta_i,\phi_i)|s_i\rangle$$

$$= L_m \quad m = 0, 1c, 1s, \ldots \quad L = S, P, D, \ldots$$

where (θ_i,ϕ_i) represents the location of the ith atom in the spherical polar coordinates, N' is a normalising constant, and C_{lm} is a modified spherical harmonic wavefunction, $C_{lm} = [4\pi/(2l + m)]^{1/2} Y_{lm}$. Consequently, the symmetry-adapted linear combinations of these

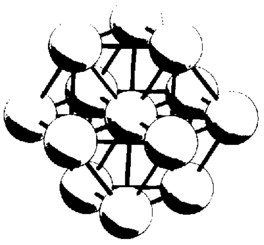

(1)

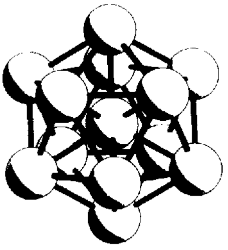

(2)

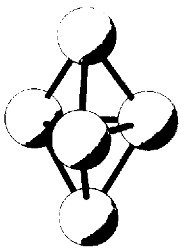

(3)

$|s_i\rangle$ for a cuboctahedron (O_h point group) are $S(a_{1g})$, $P(t_{1u})$, $D_{\pm1,2s}(t_{2g})$, $D_{0,2c}(e_g)$ and $F_{0,\pm1}(t_{1u})$ molecular orbitals. Within the Hückel approximation:

$$\langle s_i|H|\,s_j\rangle = \begin{cases} \alpha \text{ (assumed to be zero)} & i = j \\ \beta \quad i,j \text{ neighbours} & \\ 0 \quad \text{otherwise} & \end{cases}$$

The results of these interactions are shown on the left-hand side of Fig. 2. When the interstitial atom is introduced, the orbital interactions which result are illustrated in Fig. 2. The occupation of the bonding orbitals (S and P) or bonding and non-bonding orbitals (S, P and $D_{\pm1,2s}$) lead to Mulliken bond orders $p(M_s{-}M_s)$ of 3/8 and $p(M_s{-}M_c)$ of 1/4 (s and c indicate surface and central atoms), respectively. Although the individual bond order between the centered and surface atoms is smaller than that between surface atoms, the total bond order of $M_c{-}M_s$, which takes into account

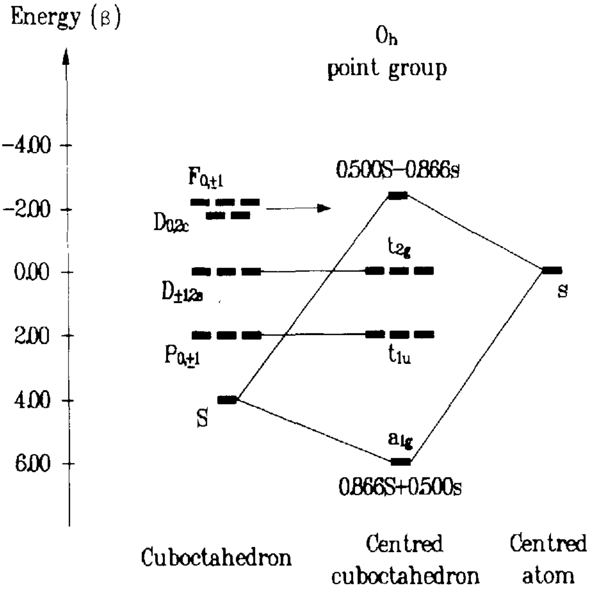

FIGURE 2 The orbital interaction diagram for a centered cuboctahedral cluster.

the differences in connectivities, $[(1/4) \times 12 = 3]$ is double that of M_s–M_s $[(3/8) \times 4 = 1.5]$.

For a centered heterometallic cuboctahedral cluster $M_{12}M'$, $\beta(M-M') = \beta(M-M) + \delta\beta$ is assumed. When the central atom is M′, the stabilization energy compared to the M_{13} cluster is:

$$\Delta E = 3 \times \delta\beta.$$

When M′ is located on the surface, the corresponding stabilization energy is:

$$\Delta E = 1.5 \times \delta\beta.$$

From this simple model, it is obvious that when $\beta(M-M') > \beta(M-M)$, the M′ atom preferentially occupies the interstitial site.

For reasons of mathematical simplicity the case of an s only model was developed above. Similar arguments are valid for those clusters where more complex basis sets are used as long as the metal–metal overlap populations are used to define the relative bonding capabilities of the surface and interstitial atoms. In general, we therefore can conclude that those atoms which have the larger metal–metal resonance integrals prefer interior to surface sites.

Ligated Clusters

(a) Where Metal–Ligand Bonding Effects Are Negligible. Extended Hückel molecular orbital calculations[26] on high nuclearity centered gold clusters of the general type $[Au(AuPR_3)_n]^{m+}$ have demonstrated that the Mulliken bond order between the central Au_c and surface Au_s, $p(Au_c-Au_s)$, is larger than that between Au_s and Au_s, $p(Au_s-Au_s)$. A model MO calculation on $[Au_{13}L_{12}]^{5+}$, where L is a two electron σ-donating ligand with orbital exponent equal to that of the P 3s orbital and an H_{ii} of −16.6 eV, with an icosahedral structure (**2**) (as a model for the cluster $[Au_{13}(PMe_2Ph)_{10}Cl_2]^{3+}$)[27] indicated that $p(Au_c-Au_s) = 0.145$, $p(Au_s-Au_s) = 0.103$ and $p(Au_s-L) = 0.271$. Since the heat of atomization of platinum [545(±21) kJ/mol][28] is greater than that for gold [379(±8) kJ/mol][28] it is reasonable to assume that

$\beta(\text{Pt–Pt}) > \beta(\text{Pt–Au}) > \beta(\text{Au–Au})$. Therefore $\delta\beta_{kl}$ is negative and from the first-order perturbation theory expression

$$\delta E = 2 \sum_{l} p_{kl}\delta\beta_{kl}$$

It is apparent that the isomer with platinum in the interstitial site is the more stable. Calculations on $[Au_{12}PtL_{12}]^{4+}$ with an icosahedral geometry have confirmed that the sum of the one electron energy for the cluster when the Pt atom is located in the center (-2022.86 eV) is lower than that when the Pt atom is located at the surface (-2021.96 eV). The magnitude of the difference (≈ 0.9 eV) is surprisingly large and underlines the importance of these differential bonding effects. It should be emphasized that although the differences in individual metal–metal bond strengths may not be large, the cumulative effect due to the large coordination number is significantly large. This suggests that the Pt atom prefers the interstitial site because the Pt–Au metal–metal interactions are larger than the Au–Au interactions. In this analysis, we have assumed that only one ligand is bonded to each surface metal atom and the Pt–L and Au–L bond strengths are essentially equal. This model provides a general basis for analyzing site preferences in clusters where the metal–ligand interactions for different metal atoms are not significantly different and metal–metal bonding predominates.

(b) Where Metal–Ligand Bonding Effects Are Significant. The effects of differential metal–ligand bonding effects on the site preferences can be understood in terms of an extended Hückel calculation on the mixed cluster $[Cu_3Fe_3L_{12}]^{3-}$ (as a model of cluster compound $[Cu_3Fe_3(CO)_{12}]^{3-}$[29]) which has a Cu_3 triangle with each edge bridged by an FeL_4 group. Two isomers of this cluster were studied. One is based on the observed structure of $[Cu_3Fe_3L_{12}]^{3}$, and the other has an inner Fe_3 triangle edge-bridged by CuL_4 groups. Figure 3 shows the total energies and Mulliken bond overlap populations for both isomers when all the bond lengths associated with the structure are kept unchanged (M–M = 2.5 Å and M–L = 2.3 Å). The significant energy difference (ca. 4 eV) between the two isomers suggests that the isomer with an inner Cu_3 triangle is much more stable than the one with an inner Fe_3 triangle.

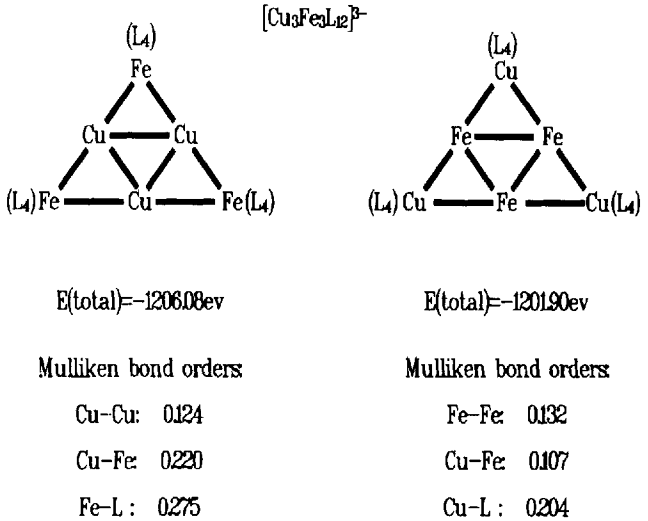

FIGURE 3 The Mulliken bond orders and the total energies for two isomers of the $[Cu_3Fe_3L_{12}]^{3-}$ cluster.

It can be seen from the figure that a significant decrease in the bond orders of M–L terminal bonds and Cu–Fe bonds results for the latter isomer. This is because there is a big difference between the Cu–L and Fe–L interactions. The strong interaction between Fe and ligands leads to the preference of Fe metal atom occupying the edge-bridging positions. This example was chosen as a particularly extreme example since the hypothetical molecule with the copper atom coordinated to four ligands would lay outside the province suggested by the noble gas rule. Nonetheless, it does emphasize the important general point that if the bonding capabilities of the metals towards ligands are very different the site preferences suggested by the metal–metal bonding trends can be overturned. More examples of these metal–ligand bonding effects will be discussed below.

(c) Clusters Without Interstitial Atoms. The isolobal relationship[30] between the BH and ML_3 fragments has provided a theoretical relationship between the borane, $B_nH_n^{2-}$, and the ligated transition metal cluster compounds. A detailed analysis of the molecular orbitals of deltahedral ligated clusters has shown that both borane and ligated metal clusters have the same number and pattern of the skeletal bonding orbitals as long as they have the same skeletal geometries. Therefore, the skeletal interaction between metal–ligand fragments can be approximately described using borane analogues. $B_5H_5^{2-}$ (trigonal bipyramidal structure (**3**)) will serve as a model for analyzing the site preferences in simple spherical clusters.

Each BH fragment contributes one σ and two $\pi(p_\Theta,p_\phi)$ fragment orbitals to the skeletal molecular orbitals, where p_Θ and p_ϕ at each vertex are defined such that they are a pair of orthogonal unit vectors which are tangential to the surface of the cluster sphere and pointing in the direction of increasing θ and ϕ, respectively. For simplicity, the σ type is assumed to be an s-like orbital rather than an s-p hybrid. The result of interaction between 5 σ's within Hückel approximations is illustrated on the left-hand side of Fig. 4. The five resultant orbitals are as follows:

		Energy
S^σ (a_1')	$0.394(\sigma_1 + \sigma_5)$ $+ 0.479(\sigma_2 + \sigma_3 + \sigma_4)$	3.646β
P_0^σ (a_2'')	$0.707(\sigma_1 - \sigma_5)$	0.000β
$P_{\pm 1}^\sigma$ (e')	$0.408(2\sigma_2 - \sigma_3 - \sigma_4)$, $0.707(\sigma_3 - \sigma_4)$	-1.000β
D_0^σ (a_1')	$0.587(\sigma_1 + \sigma_5)$ $- 0.322(\sigma_2 + \sigma_3 + \sigma_4)$	-1.646β

The linear combinations of π-sets can be obtained in terms of Stone's tensor surface harmonic expansions, which are assigned as L^π (even parity wavefunctions) and $\bar{L}^\pi$ (odd parity wavefunctions). The $\bar{L}^\pi$ tangential molecular orbitals are related to L^π orbitals by a 90° clockwise rotation of the tangential π-set (p_Θ,p_ϕ) about the radial vector at each vertex. The 5 L^π molecular orbitals are as follows:

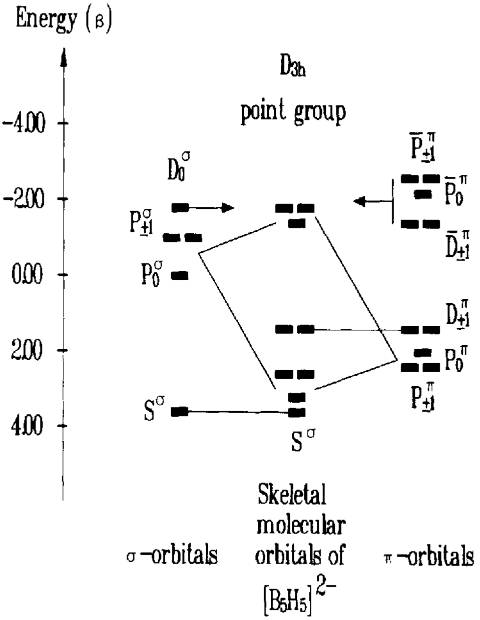

FIGURE 4 The molecular orbital energy level diagram of $[B_5H_5]^{2-}$ anion.

		Energy
P_0^π (a_2'')	$-(1/3)^{1/2}(p_{\Theta 2} + p_{\Theta 3} + p_{\Theta 4})$	2.000β
$P_{\pm1}^\pi$ (e')	$(1/14)^{1/2}[2(p_{\Theta 1} - p_{\Theta 5}) - (3)^{1/2}(p_{\Phi 3} - p_{\Phi 4})]$ $(1/14)^{1/2}[2(p_{\Phi 1} + p_{\Phi 5}) + (2p_{\Phi 2} - p_{\Phi 3} - p_{\Phi 4})]$	2.143β
$D_{\pm1}^\pi$ (e')	$(1/14)^{1/2}[2(p_{\Theta 1} + p_{\Theta 5}) - (2p_{\Theta 2} - p_{\Theta 3} - p_{\Theta 4})]$ $(1/14)^{1/2}[2(p_{\Phi 1} - p_{\Phi 5}) - (3)^{1/2}(p_{\Theta 3} - p_{\Theta 4})]$	1.551β

Within Hückel approximations and assumptions of β^σ (p − p) =

β^{π} (p − p) = β, the energy levels together with $\bar{L}^{\pi}$ molecular orbitals are shown in the right-hand side of Fig. 4.

When the mixing between L^{σ} and L^{π} is taken into account, the result is shown in Fig. 4. The mixing between L^{σ} and $\bar{L}^{\pi}$ has been ignored and assumption of β^{σ} (s − p) = β has been made to simplify the analysis. Therefore, mixing occurs between $P^{\sigma}_{\pm 1}$ and $P^{\pi}_{\mp 1}$, and also between P^{σ}_{0} and P^{π}_{0}. The bonding combinations for the above mixings are:

		Energy
$P_{\pm 1}$ (e′)	$0.351P^{\sigma}_{\pm 1} + 0.936\,P^{\pi}_{\pm 1}$	2.528β
P_{0} (a''_{2})	$0.526P^{\sigma}_{0} \pm 0.851P^{\pi}_{0}$	3.236β

Occupation of the six skeletal bonding orbitals (S^{σ}, $P^{\pi/\sigma}_{0,\pm 1}$ and $D^{\pi}_{\pm 1}$) leads to Mulliken bond orders *p*(equatorial–equatorial) of 1.072 and *p*(equatorial–axial) of 1.910. Therefore, the total bond order between the axial atom and its neighbors (5.730) is very close to that between the equatorial atom and its neighbors (5.963), and the difference is only 0.263.

From this simplified analysis it can be concluded that site preference effects arising from differences in resonance integrals ($\delta\beta$) are small for clusters where the metal atoms lie on a single spherical surface. There is only a slight preference for the atom with a larger resonance integral to occupy the higher coordination number site. The larger differences in calculated charges for the equatorial and axial sites in $B_5H_5^{2-}$ (see Fig. 1) lead to a preference for the more electronegative atom to occupy the apical site. Therefore, in such situations the first order stabilization energies associated with the differences in electronegativity and resonance integrals may be in competition and lead to a finely balanced situation.

PERIODIC TRENDS IN THE STRENGTHS OF METAL–METAL AND METAL–LIGAND INTERACTIONS

The first order perturbation theory arguments require some appreciation of the trends in resonance integrals for metal–metal interactions. Furthermore, we make the assumption that the resonance integral for a heterometallic bond M–M′ is intermediate between those for M–M and M′–M′.

Metal–Metal Interaction

For the transition metals, the metal–metal interactions can be understood in terms of the cohesive energies since crystal field splittings are not important in determining these energies.[31] The experimental values[32] of heats of vaporization of transition-series metals are plotted as a function of atomic number in Fig. 5. It can be seen that the heats of vaporization increase from first to third transition-series metals except for the IB and IIB group metals. This can be explained in terms of d orbital interactions because metal–metal bonding for transition metals arises mainly from d–d overlaps. The radial expectation values $\langle r \rangle_s$ and $\langle r \rangle_d$ for s and d

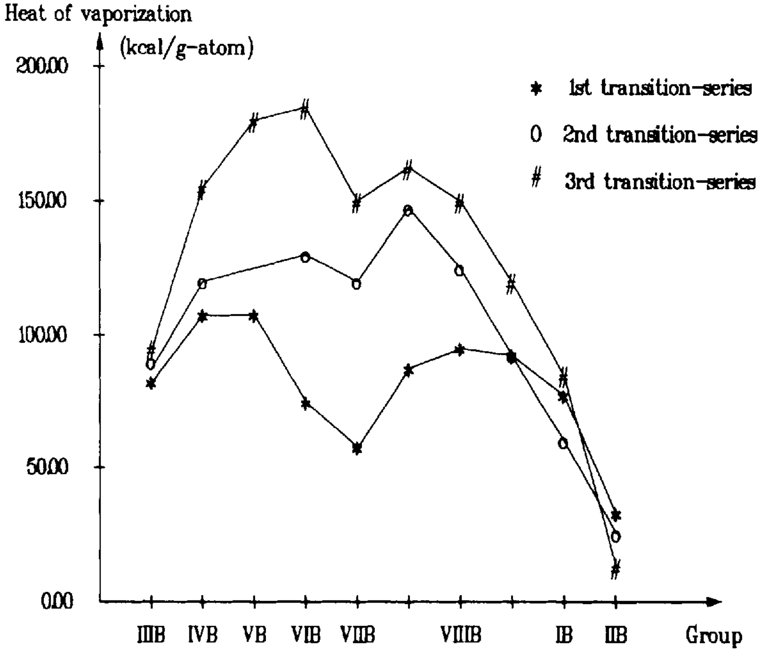

FIGURE 5 The heats of vaporization of transition-series metals as a function of group numbers.

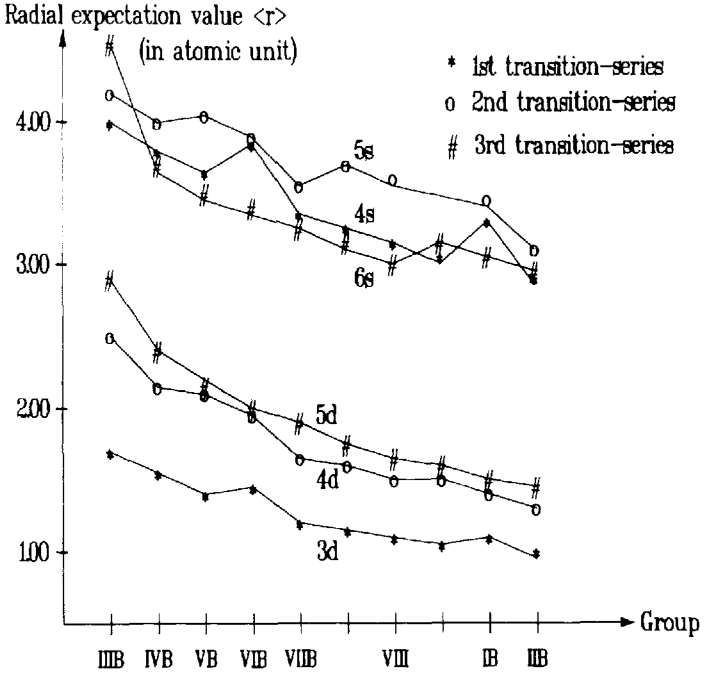

FIGURE 6 The radial expectation values for s and d valence orbitals of transition-series metals as a function of group numbers.

valence orbitals of transition-series metal atoms, which are obtained from relativistic Hartree–Fock calculations by Desclaux,[33] are plotted against group numbers in Fig. 6. It can be seen from Fig. 6 that the d orbitals are less contracted for the second and third row transition metal atoms, and consequently larger d–d overlaps result between the metal atoms. Therefore, the strength of interaction between metal atoms increases on descending a group of transition-series metals.

For the same series, metal–metal interactions for different atoms cannot be compared simply from the cohesive energies since the cohesive energies depend also on the number valence electrons involved. It is apparent from Fig. 6 that the contraction of d orbitals increases with the atomic number. Therefore, the metal–metal resonance integral is expected to decrease from left to right in the Periodic Table.

For s valence orbitals, it is apparent that the s orbital of the thrid transition-series atoms is the most contracted because of relativistic effects. For the first and second transition-series atoms, $\langle r \rangle_{5s}$ is larger than $\langle r \rangle_{4s}$ for same group atoms.

Metal–Ligand Interaction

Metal–ligand bonds are formed from interactions between ligands and metal s, p and d orbitals. The contracted nature of p valence orbitals is the same as that of d orbitals. However, the overlap between the ligand orbitals and the metal p valence orbitals decreases as the latter become more diffuse. The situation for metal–ligand interaction is therefore much more complex than that for metal–metal interactions. For the same group, the diffuse nature of the p valence orbitals increases from the first to the third transition-series metal atoms. This means that the interaction between the metal p orbitals and the ligand orbitals decreases down a transition metal group. Therefore, for late transition metal atoms, interaction between the metal and the ligand, which is mainly through the s and p orbitals of the metal atoms, is expected to decrease from lower to higher row atoms since they have very contracted d orbitals which cannot make a significant contribution to metal–ligand bonds. For early transition metal atoms, d orbitals are also involved in the metal–ligand in addition to the metal s and p valence orbitals. Therefore, a larger metal–ligand interaction is predicted for early transition metal atoms than for late transition metal atoms. These general conclusions are very important for understanding various site preferences for ligated-metal clusters which will be discussed below.

DISCUSSION

Site Preferences for Mixed Naked Clusters

The results of the arguments developed above provide a general explanation for site preferences in clusters. As indicated above, for mixed naked clusters, the atoms which have the larger resonance integrals (β) with their neighbors prefer to occupy the interior sites. For bimetallic M–Cu clusters (M: early or late transition metal atoms) the evidence from EXAFS of Cu-rich regions on the surface is consistent with the arguments developed above since the d orbitals of Cu are very contracted and energies of the p orbitals are too high to be available for metal–metal bonding. Comparing Ru and Rh, it is apparent that the metal–metal (d–d) interactions for Ru atoms are stronger than that for Rh atoms. It follows that the extent of concentration of Cu at the surface appears to be lower for Rh–Cu clusters than for Ru–Cu clusters even though the Cu/Rh and Cu/Ru atomic radius ratios are both equal to 1. This has also been confirmed by EXAFS experiments.[6]

For bimetallic clusters based on a combination of atoms of two group VIII(8–10) metals, the site preferences can be also understood through d–d interactions. Both Ir and Rh atoms are in the same group of the Periodic Table, but Ir has more diffuse d orbitals than Rh atoms because of its higher atomic number. The presence of Ir-rich at the interior region is observed for Ir–Rh clusters. For Re–Pt and Re–Pd clusters, it can be easily deduced that the interior sites are Re-rich.

For bimetallic clusters containing Cu, Ag and Au atoms, the metal–metal interactions occur mainly through s–s orbital overlaps and the filled d^{10} shell behaves in a core-like fashion. As noted above, the average radius of the s orbital follows the order $\langle r\rangle_{\mathrm{Ag}} > \langle r\rangle_{\mathrm{Cu}} > \langle r\rangle_{\mathrm{Au}}$. It can be also seen from Fig. 5 that the heats of vaporization for Cu and Au are close, but larger than Ag. Therefore, it can be concluded that the resonance integrals follow the order Au–Au ~ Cu–Cu > Ag–Ag. Consequently, there is an indication that Cu composition concentrates in the interior sites for the Cu–Ag cluster. The location of an Au-rich region in the Au–Cu clusters is less clear from the EXAFS data.[13]

When the difference in metal–metal interactions for two kinds of metals in the bimetallic clusters is not very large, the surface composition is greatly influenced by the gaseous atmosphere in contact with the clusters. This is because the gaseous molecules strongly interact with the surface metal atoms. The loss in energy on moving atoms from the interior to surface sites can be compensated for by a gain in energy in forming metal–ligand bonds. Therefore, the observation of changing site preferences for Cu–Au clusters,[13] Ag(Au)–Pd[14] and Ni–Au[15] alloys under different atmospheres can be easily understood since bonds formed between Pd (or Ni) and ligands are invariably stronger than that between

Cu (or Au) and ligands. The ligand effect on site preference will be discussed in more detailed in the following section.

For small mixed naked clusters, e.g., K_nMg and K_nAl, Mg and Al atoms prefer to occupy the centers of the clusters because the resonance integrals follow the order Al–Al > Mg–Mg > K–K. Both Mg and Al have available p orbitals for interacting with Na atoms but the p orbitals of Na are too high in energy compared to those of Mg and Al atoms to be available for bonding.

Site Preferences for Mixed Ligated Clusters

Since metal–ligand interaction is significant in site preference for mixed ligated clusters the situation for ligated clusters becomes more complicated. Examining all the structures of known mixed ligated clusters, we classify them into four types.

The first one is clusters where both the metal–metal and metal–ligand interactions are coincident for site occupations, i.e., they have larger metal–metal interaction in the interior region and also larger metal–ligand interaction at the surface sites. For example, for the clusters $[H_nNi_{38}Pt_6(CO)_{48}]^{-(6-n)}$ (n = 1 and 2)[21] and $[H_3Fe_6Pd_6(CO)_{24}]^{3-}$,[22] Pt–Pt (or Pd–Pd) bonds which are in the interior sites are stronger than Ni–Ni (or Fe–Fe) bonds, and Ni–CO (or Fe–CO) bonds which are at the surface site are stronger than Pt–CO (or Pd–CO) bonds. The latter is not too surprising in view of the way in which the d–p promotion energies of Pt (or Pd) lead to 16-electron mononuclear complexes, whereas Ni and Fe usually form 18-electron mononuclear complexes. Clusters which also belong to this type are $[Fe_3Pt_3(CO)_{15}]^{n-}$ (n = 2 and 3)[34] which have edge-bridged triangular raft structure with a Pt_3 triangle inside and $[Fe_4Pt_6(CO)_{22}]^{2-}$ [34] which has edge-bridged tetrahedral structure with a Pt_4 tetrahedron inside. Table I lists examples of this type of cluster.

The second one is clusters where metal–ligand interactions predominate the site preference effects. Most of the mixed ligated clusters which contain IB (or IIB) and VIIIB (or IIIB–VIIB) transition metals belong to this type. There is a significant difference in metal–ligand interaction between IB (or IIB) and VIIIB (or IIIB–VIIB) transition metals. The occupation of metal atoms, which have larger metal–metal and metal–ligand interactions, at

TABLE I

Examples of clusters where both the metal–metal and metal–ligand interactions are coincident for site preferences

Cluster	Description	Reference
$[H_nNi_{38}Pt_6(CO)_{48}]^{(6-n)-}$ (n = 1 and 2)	An octahedron based on fcc close packing with 4 atoms on each edge of the octahedron. The six Pt atoms form an inner octahedron at the center of the cluster.	21
$[PtRh_{12}(CO)_{24}]^{4-}$	A centered anti-cuboctahedron with a Pt atom in the center.	20
$[Pt_2Rh_{11}(CO)_{24}]^{3-}$	A centered tetracapped cube as its core with one of the Pt atoms occupying the central position.	20
$[H_3Fe_6Pd_6(CO)_{24}]^{3-}$	A hexacapped octahedron with the six Pd atoms forming an inner octahedron.	22
$[PtRh_{10}N(CO)_{21}]^{3-}$	A complex cluster core made up of a tricapped trigonal prism with two further capping atoms linking two of the prism caps. The Pt atom occupies the highest connectivity vertex in this cluster.	35
$[Pt_2Rh_9(CO)_{22}]^{3-}$	A cluster core consisting of three face-sharing octahedra. The Pt atoms occupy the highest connectivity sites.	36
$[PtRh_8(CO)_{19}]^{2-}$	Consisting of two octahedra of metal atoms sharing a triangular face. The Pt atom occupies one of the vertices in the shared face.	37
$[Fe_4Pt_6(CO)_{22}]^{2-}$	A core structure consisting of a bi-edge-bridged tetrahedron of Pt atoms with an Fe atom bridging each of the four bonds connecting the bridging atoms to the tetrahedron.	34
$[Fe_3Pt_3(CO)_{15}]^{n-}$ (n = 2 and 3)	An edge-bridged triangular raft structure with the 3 Pt atom triangle inside.	34
$[PtRh_4(CO)_4Cp_4]$	Consisting of two triangles sharing one vertex (Pt atom).	38
$[MFe_4(CO)_{16}]^{2-}$ (M = Pt and Pd)	Consisting of two triangles sharing one vertex. The Pt (or Pd) atom occupies the sharing vertex.	39

the surface sites maximize the metal–ligand interactions. Examples of clusters with triangular six-atom-raft geometries are $[Cu_3Fe_3(CO)_{12}]^{3-}$,[29] $[H_3Ag_3Rh_3(MeC(CH_2PPh_2)_3)_3]^{3+}$,[40] $H_9Cu_3Os_3(PMe_2Ph)_9$[41] and $Ir_3Pt_3(CO)_6(Cp)_3$[42] with interstitial Cu_3, Ag_3, Cu_3 and Pt_3 triangles, respectively. A tetra-capped octahedral cluster, $Hg_6Rh_4(PMe_3)_{12}$,[43] provides another example of clusters belonging to this type. The six Hg atoms form a quite regular octahedron and the Rh atoms cap four tetrahedrally related faces of this octahedron. More examples are listed in Table II. The site preference of clusters of this type is different from that of mixed naked clusters.

The third one is clusters where the metal–metal interactions predominate. There are two cases for this type of cluster. One is the case when the metal–ligand interactions for different metal atoms are roughly same. For example, for the mixed clusters $[Au_{18}Ag_{20}(PR_3)_{21}Cl_{14}]$[49] and $[Au_{13}Ag_{12}(PPh_3)_{12}Cl_6]^{m+}$ [50] (see Table III for structural descriptions), the Au atoms occupy the centers of icosahedra because the metal–metal interaction for Au metal is expected to be larger than that for Ag metal. Clusters which consist of different atoms within Group VIIIB metals or within early transition metals belong to this case. The other is the case when the metal–ligand interactions for different metal atoms are also significantly different. For example, for the cluster $[ReAu_5(PPh_3)_7H_4]^{2+}$ [51] with two tetrahedra sharing one edge, the Re atoms occupy one of the two atoms in the sharing edge. For clusters $Ru_6Cu_2(CO)_{18}(C_6H_4Me)_2$[52] (bicapped octahedron) and $Ru_4Cu_2H_2(CO)_{12}(PPh_3)_2$[53] (capped trigonal bipyramid), the Cu atom prefers to occupy the capping site with smaller connectivity.

Clusters with an interstitial main group atom belong to the fourth type (see Table IV). It has been shown that the s and p valence orbitals of an interstitial main group atom in a cluster interact extensively with the skeletal bonding orbitals derived from surface atoms in the cluster. It can be expected that a larger interaction between the interstitial atom and the skeletal atoms occurs. It is also obvious that transition metal atoms have capacities to form more metal–ligand bonds than main group atoms. Therefore, most structures of this type of clusters have an interstitial main group atom rather than have a main group atom on the skeletal surface

TABLE II

Examples of clusters where the metal–ligand interaction predominates

Cluster	Description	Reference
$[Fe_{10}Tl_6(CO)_{36}]^{6-}$	It is basd on two Fe_2Tl_3 trigonal bipyramids (the 3 Tl atoms occupy the equatorial positions) which have a further Fe atom attached to two of the Tl atoms of each bipyramid while the other two Tl atoms are linked by two bridging Fe atoms.	44
$[Hg_6Rh_4(PMe_3)_{12}]$	A tetracapped octahedron. The six Hg atoms form an inner octahedron.	43
$[Cu_6Fe_4(CO)_{16}]^{2-}$	A tetracapped octahedron. The six Cu atoms form an inner octahedron.	45
$[Ag_6Fe_3(CO)_{12}(Ph_2P)_3CH]$	A distorted tricapped octahedron. The three Fe atoms occupy the capping positions.	46
$[Os_9Hg_3(CO)_{23}]$	A plannar propellor-shaped structure based on an inner triangle of Hg atoms.	47
$[Cu_5Fe_4(CO)_{16}]^{3-}$	A "square" planner array of metal atoms with 4 Fe atoms defining the four conners of the "square" and Cu atoms at the center of each edge and in the center of the cluster.	29
$[H_9Cu_3Os_3(PMe_2Ph)_9]$	A trianglular raft structure. The 3 Cu atoms form an inner triangle with each edge of the triangle bridged by an Os atom.	41
$[Cu_3Fe_3(CO)_{12}]^{3-}$	The geometry is the same as in the above. The 3 Fe occupy the capping sites.	29
$[Ir_3Pt_3(CO)_6Cp_3]$	The geometry is the same as in the above. The 3 Pt atoms form an inner triangle and the 3 Ir atoms occupy the edge-capping positions.	42
$[M_2Ni_3(CO)_{16}]^{2}$ (M = Cr, Mo and W)	A trigonal bipyramidal structure. The 3 Ni atoms form a triangle and two $M(CO)_5$ fragments cap both sides of the triangular face.	48

TABLE III

Examples of clusters where the metal–metal interaction predominates

Cluster	Description	Reference
$[Au_{18}Ag_{20}(PR_3)_{12}Cl_{14}]$	A structure which consists of three 13-atom (Au_7Ag_6) Au-centered icosahedra sharing 3 Au vertices plus two capping Ag atoms located on the idealized 3-fold axis.	49
$[Au_{13}Ag_{12}(PPh_3)_{12}Cl_6]^{m+}$	A structure which consists of 3 interpenetrating icosahedra in line so that the 4 pentagonal rings are staggered with respect to one another. Three Au atoms occupy the 3 centers of the 3 icosahedra.	50
$[Co_3Ni_9C(CO)_{20}]$	A geometry based on a square antiprism capped on four of the triangular faces. Four Ni atoms occupy the capping positions.	54
$[Co_6Ni_2C_2(CO)_{10}]^{2-}$	A cluster core which consists of two trigonal prisms sharing a square face with a C atom at the center of each prism. The Ni atoms occupy two 3-connected sites.	55
$[Rh_6Ni(CO)_{16}]^{2-}$	An octahedron is capped by a Ni atom.	56
$[Os_3Ni_3Cp_3(CO)_9]$	A bicapped tetrahedron. Two Ni atoms occupy the Os_3 face and one of the Os_2Ni faces.	57
$[Os_6Pt_2(CO)_{17}(C_8H_{12})_2]$	A bicapped octahedron. Pt atoms occupy the capping positions.	58
$[Re_8In_4(CO)_{32}]$	A tetrahedron of Re atoms with an $InRe(CO)_5$ unit capping each face of the tetrahedron.	59
$[ReAu_5(PPh_3)_7H_4]^{2+}$	A geometry with two tetrahedra sharing one edge. Re atoms occupy one vertex of the sharing edge.	51
$[Ru_6Cu_2(CO)_{18}(C_6H_4Me)_2]$	A para-bicapped octahedron with Cu atoms occupying the capping sites.	52
$[Ru_4Cu_2H_2(CO)_{12}(PPh_3)_2]$	A capped trigonal bipyramid with one Cu occupying one of Ru_2Cu triangular face.	53

TABLE IV

Examples of clusters with a main group interstitial atom

Cluster	Description	Reference
$[Ru_6C(CO)_{17}]$	An octahedron	17
$[Rh_6N(CO)_{15}]^-$	A trigonal prism	60
$[Co_6N(CO)_{15}]^-$	A trigonal prism	61
$[Re_7C(CO)_{21}]^{3-}$	A capped octahedron	62
$[Re_8C(CO)_{24}]^{2-}$	A bicapped octahedron	63
$[Rh_8C(CO)_{19}]$	A square antiprism	64
$[Co_8C(CO)_{18}]^{2-}$	A square antiprism	65
$[Rh_9P(CO)_{21}]^{2-}$	A capped square antiprism	66
$[Rh_{10}S(CO)_{22}]^{2-}$	A bicapped square antiprism	18
$[Os_{10}C(CO)_{24}]^{2-}$	A tetracapped octahedron	67
$[Rh_{12}Sb(CO)_{27}]^{3}$	An icosahedron	19

and a metal atom in the interstitial site. Of course, the size effect is also significant for site preferences and will not be discussed in this paper.

Some simple clusters do not have site preferences as in those examples discussed above. As indicated above for the $B_5H_5^{2-}$ cluster, the total Mulliken overlaps for equatorial and axial sites with their neighbors are very close. No site preference is predicted for trigonal bipyramidal transition metal clusters as long as the metal–ligand interactions for different metal atoms are similar. For example, the clusters $[PtRh_4(CO)_{12}]^{2-}$ [68] and $[PtIr_4(CO)_{12}]^{2-}$,[69] which have the same number of skeletal electron pairs as $B_5H_5^{2-}$ (6, i.e., $n + 1$), have the Pt atom occupying the axial position. In the former example, although the Pt atom is predicted to have a larger metal–metal interaction than the Rh atom (see cluster $[PtRh_{12}(CO)_{24}]^{4-}$ [20] in the first type) it does not occupy the equatorial position. For the clusters $[PtRh_4(CO)_{14}]^{2-}$ [68] and $[PtIr_4(CO)_{14}]^{2-}$ [69] with 2 more electron pairs, the $\bar{D}^{\pi}_{\pm 1}$ antibonding molecular orbitals are now occupied. The occupation of $\bar{D}^{\pi}_{\pm 1}$ leads to an increase in the bond order between equatorial atoms [p(equatorial–equatorial) = 1.357] and a decrease between axial and equatorial atoms [p(axial–equatorial) = 1.340] because the $\bar{D}^{\pi}_{\pm 1}$ orbitals have antibonding character between axial and equatorial atoms and bonding character between equatorial atoms. The Pt atom in both clusters occupies the equatorial position, although in the latter example Ir atoms are predicted to have a larger metal–metal interaction than the Pt atom since the Ir is located on the left-hand side of Pt in the Periodic Table. Other examples are the clusters $[FeIr_4(CO)_{15}]^{2-}$ with 76 electrons and $[Fe_2Ir_3(CO)_{14}]^-$ with 72 electrons.[70] In both clusters, the Fe atoms occupy the axial positions of the trigonal bipyramid. Clusters $[RuRh_4(CO)_{15}]^{2-}$ [71] and $[RuIr_4(CO)_{15}]^{2-}$ [72] with a trigonal bipyramidal structure, in which Ru occupies the axial position, provide additional examples for this situation.

In summary, the site preferences for naked clusters depend only on the strength of metal–metal interaction; metal atoms which have larger metal–metal interactions prefer to occupy the interior sites or the sites of larger connectivities. For ligated clusters, metal–ligand interactions are significant in influencing the site preferences, but in many cases the metal–metal interactions provide the dominant interaction.

Acknowledgments

The S.E.R.C. and the Chinese Academy of Sciences are thanked for their financial support and Dr. Tom Slee for helpful discussions.

References

1. B. F. G. Johnson and J. Lewis, Adv. Inorg. Chem. Radiochem. **24**, 225 (1981); B. F. G. Johnson and J. Lewis, Phil. Trans. Roy. Soc. London A **308**, 5 (1982).
2. E. L. Muetterties, T. N. Rhodin, E. Band, C. F. Brucker and W. R. Pretzer, Chem. Rev. **29**, 91 (1979); E. L. Muetterties and R. M. Wexler, *Survey Prog. Chem.* **10**, 61 (1983).
3. R. Whyman, in *Transition Metal Clusters*, ed. B. F. G. Johnson (Wiley, New York, 1981), Chapter 8, p. 545; R. Whyman, Phil. Trans. Roy. Soc. London A **308**, 131 (1982).
4. M. M. Kappers, Chem. Rev. **88**, 369 (1988).
5. J. C. Phillips, Chem. Rev. **86**, 619 (1986).
6. J. H. Sinfelt, Acc. Chem. Res. **20**, 134 (1987) and references therein.
7. D. M. P. Mingos, Chem. Soc. Rev. **15**, 31 (1986); D. M. P. Mingos and R. L. Johnston, Structure and Bonding, **68**, 29 (1987); D. M. P. Mingos and D. J. Wales, *Introduction to Cluster Chemistry* (Prentice-Hall, to be published).
8. A. J. Stone, Mol. Phys. **41**, 1339 (1980); Inorg. Chem. **20**, 563 (1981); Polyhedron **3**, 1229 (1984).
9. I. Boustani, W. Pewestorf, P. Fantucci, V. Bonacic-Koutecky and J. Koutecky, Phys. Rev. B **35**, 9437 (1987); V. Bouacic-Koutecky, P. Fantucci and J. Kou-

tecky, Phys. Rev. B **37**, 4369 (1988); J. Koutecky, V. Bouacic-Koutecky, I. Boustani and P. Fantucci, in *Large Finite Systems*, eds. J. Jortner *et al.* (D. Reidel Publishing Company, 1987, p. 303.

10. B. K. Rao and P. Jena, Phys. Rev. B **37**, 2867 (1988); B. K. Rao, S. N. Khanna and P. Jena, Z. Phys. D **3**, 219 (1986).
11. W. D. Knight, K. Clemenger, W. A. De Heer, W. Saunders, M. Y. Chou and M. L. Cohen, Phys. Rev. Lett. **52**, 2141 (1984); W. D. Knight, K. Clemenger, W. A. De Heer and W. Saunders, *Sol. State Commun.* **53**, 445 (1985).
12. F. F. Abraham and C. R. Brundle, J. Vac. Sci. Technol. **18**, 506 (1981).
13. G. Meitzner, G. H. Via, F. W. Lytle and J. H. Sinfelt, J. Chem. Phys. **78**, 2533 (1983).
14. R. Bouwman, G. J. M. Lippits and W. M. H. Sachtler, J. Catalysis **25**, 350 (1972).
15. F. L. Williams and M. Boudart, J. Catalysis **30**, 438 (1973).
16. M. M. Kappes, M. Schür, P. Radi and E. Schumacher, Chem. Phys. Lett. **119**, 11 (1985); M. M. Kappes, M. Schür and E. Schumacher, J. Phys. Chem. **91**, 658 (1987).
17. A. Sirugi, M. Bianchi and E. Benedetti, J. Chem. Soc., Chem. Commun. 596 (1969).
18. G. Ciani, L. Garlaschelli, A. Sironi and S. Martinengo, J. Chem. Soc., Chem. Commun. 536 (1981).
19. A. Fumagalli, S. Martinengo and G. Ciani, J. Chem. Soc., Chem. Commun. 1381 (1983).
20. A. Fumagalli, S. Martinengo and G. Ciani, J. Chem. Soc., Chem. Commun. 1831 (1983).
21. A. Ceriotti, F. Demartin, G. Longoni, M. Manassero, M. Marchionna, G. Piva and M. Sansoni, Agnew. Chem. Int. Ed. Engl. **24**, 697 (1984).
22. G. Longoni, M. Manassero and M. Sansoni, J. Amer. Chem. Soc. **102**, 3242 (1980).
23. A. Streitwieser, Jr., *Molecular Orbital Theory for Organic Chemists* (John Wiley & Sons, Inc., New York, London, 1961).
24. J. J. Ott and B. M. Gimarc, J. Amer. Chem. Soc. **108**, 4303 (1986).
25. C. A. Coulson and H. C. Longuet-Higgins, Proc. Roy. Soc. A **191**, 39 (1947).
26. K. P. Hall, D. I. Gilmour and D. M. P. Mingos, J. Organomet. Chem. **268**, 275 (1984).
27. C. E. Briant, B. R. C. Theobald, J. W. White, L. K. Bell, A. J. Welch and D. M. P. Mingos, J. Chem. Soc., Chem. Comm. 201 (1981).
28. N. N. Greenwood and A. Earnshaw, *Chemistry of the Elements* (Pergamon Press, Oxford, New York, Toronto, Sydney, Paris and Frankfurt, 1984), pp. 1333 and 1368.
29. G. Doyle, K. A. Eriksen and D. Van Engen, J. Amer. Chem. Soc. **108**, 445 (1986).
30. R. Hoffmann, Nobel Lecture 1981, Science **221**, 995 (1981); R. Hoffmann, Angew. Chem. Int. Ed. Engl. **21**, 711 (1982).
31. J. S. Griffith, J. Inorg. Nucl. Chem. **3**, 15 (1956).
32. R. A. Williams, *Handbook of the Atomic Elements* (Vision Press Limited, British Commonwealth, 1971).
33. J. P. Desclaux, Atomic Data and Nuclear Data Tables **12**, 311 (1973).
34. G. Longoni, M. Manassero and M. Sansoni, J. Amer. Chem. Soc. **102**, 7973 (1980).
35. S. Martinengo, G. Ciani and A. Sironi, J. Amer. Chem. Soc. **104**, 328 (1982).
36. A. Fumagalli, S. Martinengo and G. Ciani, J. Organomet. Chem. **273**, C46 (1984).

37. A. Fumagalli, S. Martinengo, G. Ciani and G. Marturano, Inorg. Chem. **25**, 592 (1986).
38. M. Green, J. A. K. Howard, R. M. Mills, G. N. Pain, F. A. G. Stone and P. Woodward, J. Chem. Soc., Chem. Commun. 867 (1981).
39. G. Longoni, M. Manassero and M. Sansoni, J. Amer. Chem. Soc. **102**, 3242 (1980).
40. F. Bochechi, J. Ott and L. M. Venanzi, J. Amer. Chem. Soc. **107**, 1760 (1985).
41. T. H. Lemmen, J. C. Huffman and K. G. Coulton, Angew. Chem. Int. Ed. Engl. **25**, 262 (1986).
42. M. J. Freeman, A. D. Miles, M. Murray, A. G. Orpen and F. A. G. Stone, Polyhedron, **3**, 1093 (1984).
43. R. A. Jones, F. M. Real, G. Wilkinson, A. M. R. Galas and M. B. Hursthouse, J. Chem. Soc., Dalton Trans. 126 (1981).
44. K. H. Whitmire, R. R. Ryan, H. J. Wasserman, T. A. Albright and Sung-Kwon Kang, J. Amer. Chem. Soc. **108**, 6831 (1986).
45. G. Doyle, K. A. Eriksen and D. Van Engen, J. Amer. Chem. Soc. **107**, 7914 (1985).
46. C. E. Briant, R. G. Smith and D. M. P. Mingos, J. Chem. Soc., Chem. Commun. 586 (1984).
47. M. Fajardo, H. D. Holden, B. F. G. Johnson, J. Lewis and P. R. Raithby, J. Chem. Soc., Chem. Commun. 24 (1984).
48. J. K. Ruff, R. P. White and L. F. Dalh, J. Amer. Chem. Soc. **93**, 2159 (1971).
49. B. K. Teo, M. Hong, H. Zhang, D. Huang and X. Shi, J. Chem. Soc., Chem. Commun. 204 (1988).
50. B. K. Teo and K. Keating, J. Amer. Chem. Soc. **106**, 2224 (1984).
51. P. D. Boyle, B. J. Johnson, A. Buehler and L. H. Pignolet, Inorg. Chem. **25**, 7 (1986).
52. J. S Bradley, G. B. Ansell and M. A. Modrick, Acta. Cryst. C **40**, 365 (1984).
53. M. J. Freeman, M. Green, A. G. Orpen, I. D. Slater and F. A. G. Stone, J. Chem. Soc., Chem. Commun. 1332 (1983).
54. A. Ceriotti, P. R. Della, G. Longoni, M. Manassero and M. Sansoni, J. Chem. Soc., Dalton Trans. 1181 (1984).
55. A. Arrigoni, A. Ceriotti, P. R. Della, G. Longoni, M. Manassero, N. Masciocchi and M. Sanasoni, Angew. Chem. Int. Ed. Engl. **23**, 322 (1984).
56. A. Fumagalli, G. Longoni, P. Chini, A. Albinati and S. Bruckner, J. Organomet. Chem. **202**, 329 (1980).
57. E. Sappa, M. Lanfranchi, A. Tiripicchio and M. Y. Camellini, J. Chem. Soc., Chem. Commun. 995 (1981).
58. C. Couture, D. H. Farrar and R. J. Goudsmit, Inorg. Chim. Acta. **89**, L29 (1984).
59. H. J. Haupt and H. Preut, Acta. Cryst. B **35**, 1205 (1979).
60. R. Bonfichi, G. Ciani, A. Sironi and S. Martinengo, J. Chem. Soc., Dalton Trans. 253 (1983).
61. S. Martinengo, G. Ciani, A. Sironi, B. T. Heaton and J. Mason, J. Amer. Chem. Soc. **101**, 7095 (1979).
62. G. Ciani, G. D'Alfonso, M. Freni, P. Romiti and A. Sironi, J. Chem. Soc., Chem. Commun. 339 (1982).
63. G. Ciani, G. D'Alfonso, M. Freni, P. Romiti and A. Sironi, J. Chem. Soc., Chem. Commun. 705 (1982).
64. V. G. Albano, M. Sansoni, P. Chini, S. Martinengo and D. Strumolo, J. Chem. Soc., Dalton Trans. 305 (1975).
65. V. G. Albano, P. Chini, S. Martinengo, M. Sansoni, D. Strumolo and G. Ciani, J. Chem. Soc., Dalton Trans. 463 (1978).

66. J. L. Vidal, W. E. Walker, R. L. Pruett and R. C. Schoening, Inorg. Chem. **18**, 129 (1979).
67. P. F. Jackson, B. F. G. Johnson, J. Lewis, W. J. H. Nelson and M. McPartlin, J. Chem. Soc., Dalton Trans. 2099 (1982).
68. A. Fumagalli, S. Martinengo, P. Chini, D. Galli, B. T. Heaton and R. D. Pergola, Inorg. Chem. **23**, 2947 (1984).
69. A. Fumagalli, R. D. Pergola, F. Bonacina, L. Garlaschelli, M. Moret and A. Sironi, J. Amer. Chem. Soc. **111**, 165 (1989).
70. R. D. Pergola, L. Garlaschelli, F. Demartin, M. Manassero, N. Masciocchi, M. Sansoni and A. Fumagalli, J. Chem. Soc., Dalton Trans. 1109 (1989).
71. A. Fumagalli and G. Ciani, J. Organomet. Chem. **272**, 91 (1984).
72. A. Fumagalli, T. f. Koetzle and F. Takusagawa, J. Organomet. Chem. **213**, 365 (1981).